How to cite: *Angew. Chem. Int. Ed.* **2022,** *61,* e202112638
International Edition: doi.org/10.1002/anie.202112638
German Edition: doi.org/10.1002/ange.202112638

Corannulenes

Diazapentabenzocorannulenium: A Hydrophilic/Biophilic Cationic Buckybowl

Qiang-Qiang Li[+], Yosuke Hamamoto[+], Germain Kwek, Bengang Xing, Yongxin Li, and Shingo Ito**

Abstract: *Polycyclic aromatic molecules are promising functional materials for a wide range of applications, especially in organic electronics. However, their largely hydrophobic nature has impeded further applications. As such, imparting high solubility/hydrophilicity to polycyclic aromatic molecules leads to a breakthrough in this research field. Herein, we report the synthesis of diazapentabenzocorannulenium, a cationic nitrogen-embedded buckybowl bearing a central imidazolium core, by a bottom-up strategy from polycyclic aromatic azomethine ylide. X-ray crystallography analyses have revealed a bowl-shaped molecular structure that is capable of forming charge-segregated one-dimensional columns by bowl-in-bowl packing. In addition to its fluorescence capabilities and high dispersibility in water, the molecule was found to selectively localize in the mitochondria of various tumor cells, showing potential as viable mitochondria-selective fluorescent probes.*

Polycyclic aromatic molecules are one of the most important class of organic molecules owing to their widespread applications in various scientific fields.[1–5] The significant progress and application of polycyclic aromatic molecules in material sciences, especially in organic electronics, are mainly based on their intrinsic hydrophobic properties.[6,7] In order to further extend possible applications, for example in biological or medicinal research, the development of highly-soluble/hydrophilic molecules is desirable.[8,9] The most conventional method to achieve water-soluble polycyclic aromatic molecules is to add hydrophilic substituents at their peripheral positions (Figure 1a).[10–16] However, the method may not be ideal in terms of step economy as it requires some additional steps for functionalization. It is therefore essential to develop more efficient methods in introducing hydrophilicity to polycyclic aromatic molecules by other methods than introducing hydrophilic substituents. A possible solution would be to change the framework of polycyclic aromatic molecules. Firstly, the introduction of curvature to planar framework would be an efficient method to change the degree of intermolecular interaction and aggregation, resulting in higher solubility (yellow in Figure 1b).[17–20] Secondly, adding positive or negative charges into polycyclic aromatic molecules will increase ionic solvation potentials, which lead to better solvation of ions (red in Figure 1b).[21] Lastly, introducing heteroatoms will help improve molecular polarity and increase affinity with polar solvents (blue in Figure 1b).[20,22–26] Although these three concepts themselves are not new, with such modifications, polycyclic aromatic molecules can be conferred higher solubility and hydrophilic functions required for biological and supramolecular applications.

Considering the abovementioned factors, cationic curved polycyclic aromatic molecules have attracted much attention as they will have physical and chemical properties different from neutral planar molecules. An effective method in generating cationic curved polycyclic aromatic molecules is chemical oxidation of neutral molecules using external oxidants.[27–31] However in this work, we have adopted a different approach in generating cationic curved polycyclic aromatic molecules via introducing intrinsically stable cationic functionality into polycyclic aromatic structures.[32–34] Herein, we utilized imidazolium, which is an important structural motif for functional organic materials such as ionic liquids[35–37] and N-heterocyclic carbene precursors.[38–40]

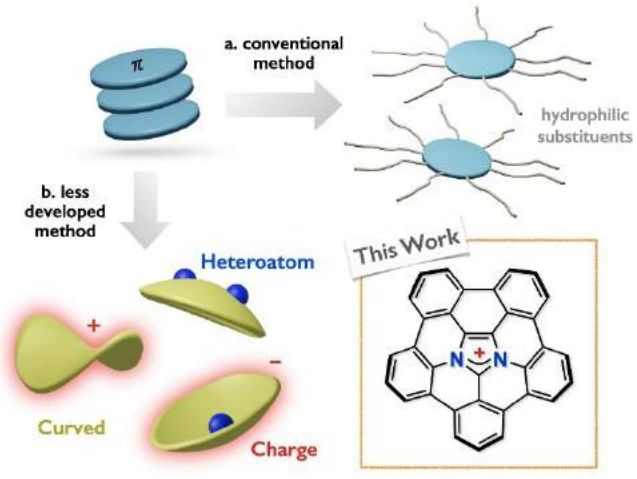

Figure 1. a) A conventional method to increase solubility/hydrophilicity to polycyclic aromatic molecules: introduction of hydrophilic substituents. b) Less developed methods: introduction of curvature, charge, and heteroatoms to polycyclic aromatic molecules.

[*] Dr. Q.-Q. Li,[+] Y. Hamamoto,[+] G. Kwek, Prof. Dr. B. Xing, Dr. Y. Li, Prof. Dr. S. Ito
Division of Chemistry and Biological Chemistry
School of Physical and Mathematical Sciences
Nanyang Technological University
21 Nanyang Link, Singapore 637371 (Singapore)
E-mail: Bengang@ntu.edu.sg
sgito@ntu.edu.sg

[+] These authors contributed equally to this work.

Despite its potential utility and application, imidazolium-containing polycyclic aromatic molecules are limited.[41,42] Here we report the synthesis of diazapentabenzocorannulenium, a cationic bowl-shaped polycyclic aromatic molecule bearing multiple internal nitrogen atoms. This molecule exhibits fluorescence and high solubility in various solvents including water. In addition, the molecule selectively localized at the mitochondria of tumor cells, showing potential as mitochondrial fluorescent probes.

As shown in Scheme 1, the synthesis of diazapentabenzocorannulenium **4** started with 1,3-dipolar cycloaddition of 6-chlorophenathridine **1** and polycyclic aromatic azomethine ylide prepared from iminium salt **2**, which proceeds via a nitrilium salt intermediate generated at high temperature under basic conditions.[43,44] The subsequent dehydrogenation took place spontaneously to form fused imidazolium salt **3**, the structure of which was confirmed by X-ray crystallography analysis (Figure S8). The access to diazapentabenzocorannulenium **4a** was accomplished by palladium-catalyzed intramolecular cyclization, where the use of triphenyl phosphine and potassium carbonate is essential to obtain a high yield (11%) of **4a**, although the reaction produced a lot of side products that could not be identified. Unfortunately, as **4a** resisted all attempts at crystallization, an anion exchange reaction of **4a** was attempted with silver hexafluoroantimonate ($AgSbF_6$) in methanol to obtain the corresponding hexafluoroantimonate salt **4b**. Single crystals of **4b** suitable for X-ray crystallography analysis were obtained by slow diffusion of 1,3-difluorobenzene to a solution of **4b** in methanol under argon at room temperature. It crystallized in monoclinic space group $P2_1/c$ and composed of four ionic pairs of **4b** including solvent molecules. The X-ray diffraction analysis elucidated that **4b** has a bowl-shaped structure with bowl depths of 0.97–1.43 Å (Figure 2a). This bowl depth value is larger than the other closed-shell cationic buckybowls reported in literature, such as "hydrazinobuckybowl" (ca. 0.7 Å)[28] and BN-substituted triangulene (0.07–0.25 Å).[34] On the other hand, these values are ca. 0.4 Å shorter than the parent azapentabenzocorannulene (1.38–1.73 Å).[45] This shallower bowl depth is attributed to shorter C–N bonds than C–C bonds. The bowl inversion energy was determined by density functional theory (DFT) calculation at the B3LYP/6-311+G(2d,p) level of theory to be 8.5 kcal mol^{-1}, which is lower than the azapentabenzocorannulene (17.0 kcal mol^{-1}) (Figure S14).

Another notable feature of **4b** in the crystal structure is the formation of charge-segregated one-dimensional col-

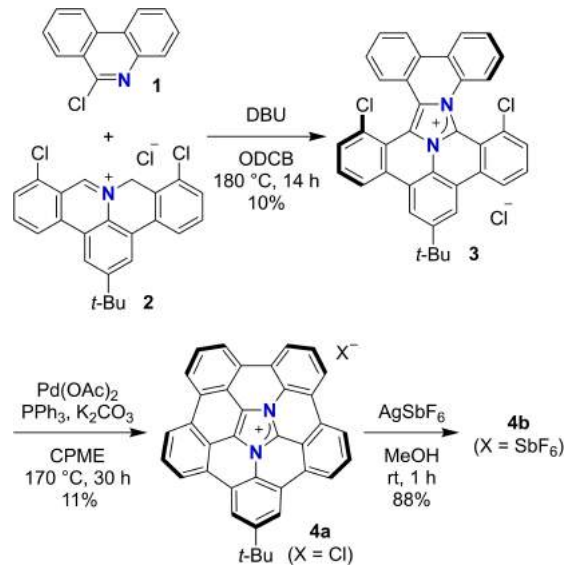

Scheme 1. Synthesis of diazapentabenzocorannulenium **4**.

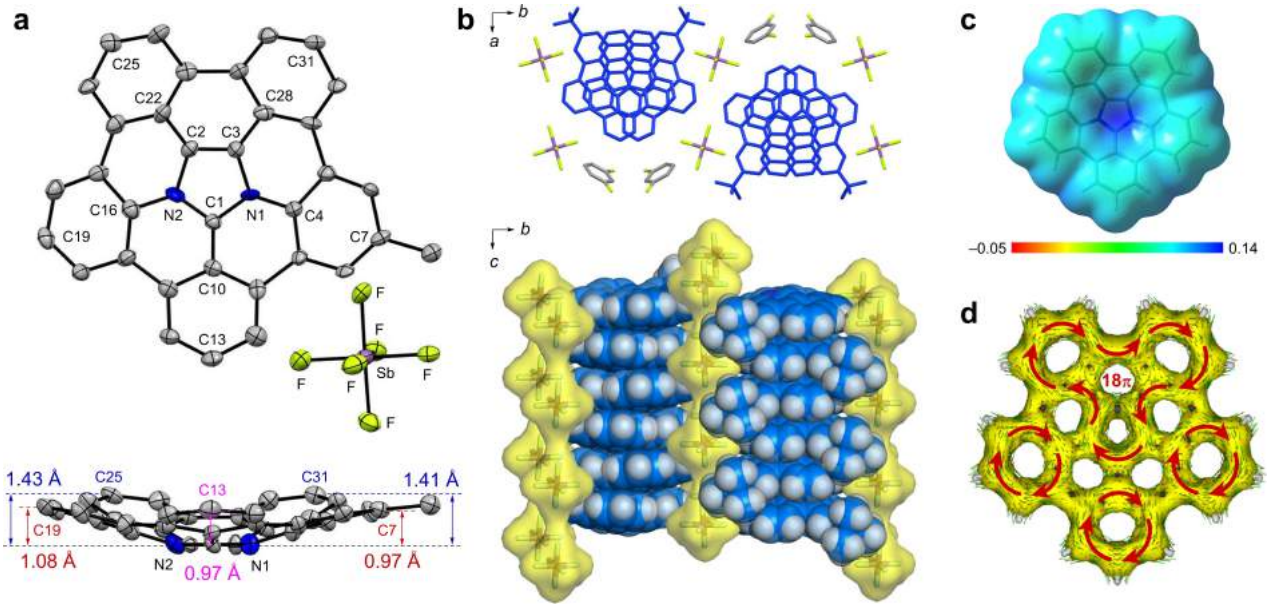

Figure 2. a) ORTEP structure of **4b** with thermal ellipsoids at 50% probability. The hydrogen atoms and the methyl groups of *tert*-butyl group are omitted for clarity. b) Packing structure of **4b**. c) Electrostatic potential map of **4**. d) ACID plot of **4**.

umns along to the *c* axis by intermolecular bowl-in-bowl interaction (Figure 2b). This indicates that the intermolecular concave-to-convex interaction is more favorable than the intermolecular repulsion between positive charges over the entire molecule. Each molecule in the column is shifted by about 82° so that the *tert*-butyl groups can fill the vacant space complementarily with 1,3-difluorobenzene and the counterion species. The intermolecular stacking distance of 3.54 Å is closer than neutral azapentabenzocorannulene (3.69 Å).[45] Meanwhile, the central imidazolium rings are "slipped stacked" with 29.8° degrees (Figure S11), in contrast to azapentabenzocorannulene core being overlapped.[45] The electrostatic potential map shown in Figure 2c indicates that this may be attributed to interaction between the relatively positive imidazolium core and the relatively negative benzene rings. The adjacent columns were concave-to-convex π-stacking with dipoles in opposite directions in order to cancel overall dipole moments. It is worth noting that the formation of charge-segregated column by heteroatom-containing polycyclic aromatic molecules has been reported, but most examples have planar or quasi-planar structures,[31,46–48] Therefore, this molecule is one of the rare examples of cationic buckybowls forming highly ordered charge-segregated one-dimensional columns,[49] which are expected to be applied as charge-transfer materials with high carrier density.[50]

The aromaticity of **4** was evaluated by nucleus-independent chemical shift (NICS) analysis and the anisotropy of the induced current density (ACID) using DFT calculations at the B3LYP/6-311+G(2d,p) level of theory. The imidazolium ring and the peripheral five benzene rings show NICS(0) values of −14.9 ppm and −7.6 to −8.0 ppm, respectively (Figure S20), suggesting that the aromatic contribution in the central imidazolium ring and the outer five benzene rings is significant, which is similar to azapentabenzocorannulene.[45] The ACID plot also supports the presence of 6π conjugation on the imidazolium and five benzene rings, while another clockwise ring current in the 18π ring including the central imidazolium and three peripheral benzenes is also observed as a minor contribution (Figure 2d).

During our experimental investigation, imidazolium salt **4a** possessing a chloride ion was found to exhibit high solubility in common polar reagents such as acetonitrile, dimethylsulfoxide, and methanol, whereas **4b** possessing a hexafluoroantimonate ion shows much lower solubility. Moreover, **4a** also gave a clear yellow "solution" in water despite the absence of hydrophilic substituents. As such, further investigations were performed to elucidate the phenomenon in water. Dynamic light scattering (DLS) (Figure 3d) revealed the presence of **4a** nanostructures in water with an average size of 38 nm. Transmission electron microscope (TEM) images further confirmed a uniform spherical morphology (Figure 3a,b) with a size distribution (36.7±3.0 nm; Figure 3c) matching that of the DLS data. These results have revealed that **4a** is highly dispersed in water to give a visually clear and transparent suspension. This was also supported by the Tyndall effect observed from **4a** in water (Figure 3d).

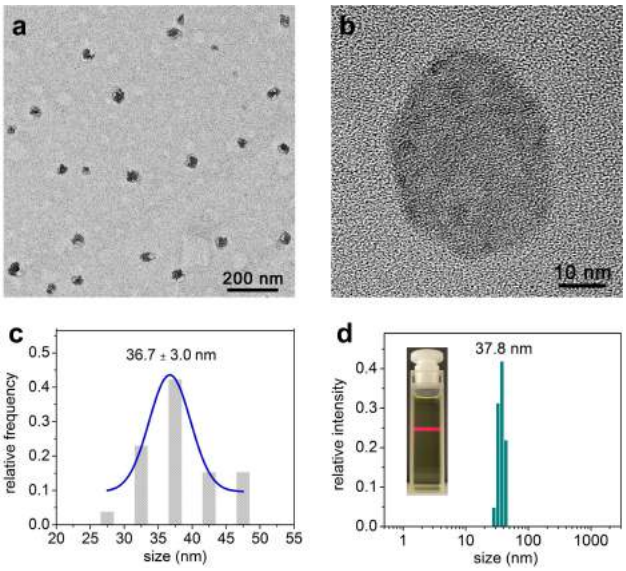

Figure 3. a) Low magnification TEM image of **4a**. b) High magnification TEM image of **4a**. c) Size distribution of **4a** determined by TEM analysis. d) Size distribution of **4a** in aqueous suspension determined by DLS analysis. Inset: photo of aqueous suspension of **4a** irradiated with red laser.

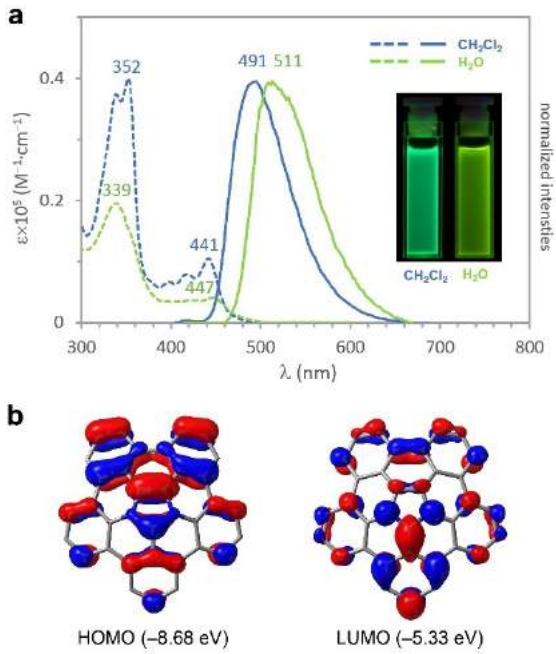

Figure 4. a) UV-visible absorption and normalized emission spectra (excited with 400 nm) of **4a** (2.0×10^{-5} M) in dichloromethane (CH_2Cl_2) and water (H_2O). b) HOMO and LUMO of **4** (iso value = 0.030).

To study the fluorescence capabilities of **4a**, the absorption and emission spectra in dichloromethane and water were obtained. As shown in Figure 4a, a solution of **4a** in dichloromethane exhibits broad absorption at $\lambda = 300$–500 nm with discrete major peaks at 352, 441 nm, which are slightly lower than those of the azapentabenzocorannulene

(395 and 466 nm).[45] In contrast, its aqueous suspension showed broaden absorption bands with peaks at 339 and 447 nm. The lower intensity could be attributed to the formation of nanoparticles in water, which is known to be a common phenomenon.[51–53] To assign the absorption bands in the absorption spectra, time-dependent DFT calculations were performed at the B3LYP/6-311+G(2d,p) level of theory. The low band at 441 nm is attributed to the transition from HOMO (−8.68 eV) to LUMO (−5.33 eV) (Figure 4b) with an oscillator strength of 0.1464 (Table S3). The HOMO of **4** is mainly delocalized at the side of the 18π conjugation including the central imidazolium core. In contrast, the LUMO is localized centered at C1 to the benzene ring at its tip. A noteworthy feature in the fluorescence spectra is solvatofluorchromic behavior: the emission of **4a** in dichloromethane and water appeared at 491 and 511 nm, respectively, with fluorescent quantum yields of 12% and 6%. The aqueous suspension exhibited obvious red shift compared with dichloromethane solution. Considering the polarity of organic solvents does not affect the emission wavelengths (Figure S12), this difference would be attributed to the aggregation of **4a** in water.

The fluorescent properties and high dispersibility of **4a** in water motivated us to further investigate its potential biological applications. We first assessed the biocompatibility of imidazolium **4a** with a resazurin based toxicology assay kit. HeLa, HCT116, and MDA-MB-231 cells were incubated with **4a** for 24 h. The incubation did not cause any drastic effect on the viabilities of the various treated cell lines, indicating relatively low toxicity of **4a** (Figure S24). Subsequently, HeLa cells incubated with **4a** were co-stained with CellMask™ Deep Red Plasma (Figure 5a). Fluorescence emission of **4a** upon excitation at 488 nm was observed inside the cytoplasm, which clearly indicates the successful cellular uptake of **4a** after 2 h incubation.

Upon confirming successful cellular uptake, we hypothesized that the unique cationic core present in **4a** might confer it certain specific subcellular localization properties, particularly in the mitochondria due to possible affinity with its negative membrane potential (−160 to −180 mV).[32,33,54] In order to further confirm this, HeLa, HCT116, and MDA-MB-231 cells incubated with **4a** were co-stained with MitoTracker™ Red FM to observe the extent of possible co-localization. As shown in Figure 5b, the merged confocal images of MitoTracker™ Red FM and **4a** showed significant overlap for all the tested cell lines. These results have confirmed that **4a** mainly accumulates in the mitochondria upon cellular uptake. The high selectivity could be explained by an appropriate balance of lipophilicity and cationic nature of **4a**. Lipophilicity of **4a** was determined via a shake-flask method[55] with a log *P* value of 1.15±0.05 (Table S10). This indicates that **4a** possesses good lipophilicity to pass through membranes. Given its positive charge, as shown in the electrostatic potential map in Figure 2c, the cationic nature of **4** plays an important role in its selective mitochondrial accumulation. Compared to conventional small molecule mitochondrial targeting strategies, our polycyclic aromatic molecule does not require further lipophilic and cationic conjugations to confer it efficient mitochondrial targeting properties. Therefore, our molecule could be potentially used as a mitochondria-selective fluorescent probe to complement the known probes.[56]

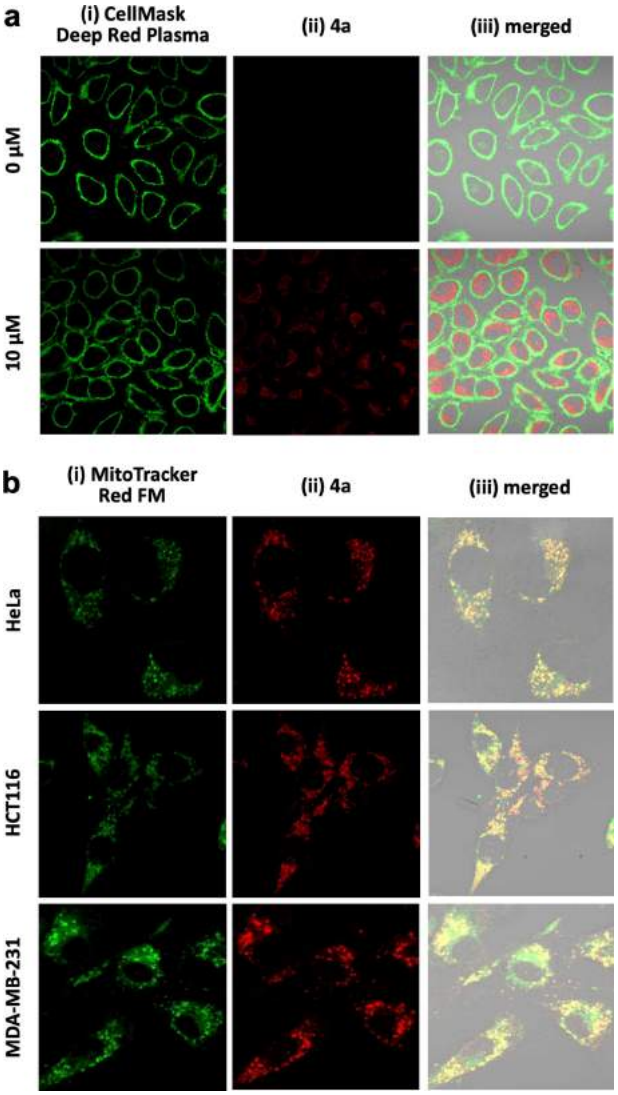

Figure 5. a) Confocal fluorescence images of HeLa cells stained with CellMask Deep Red Plasma (5 μg mL^{-1}) and **4a** (0–10 μM). Images of (i) CellMask Deep Red Plasma (excited with 640 nm laser) and (ii) **4a** (excited with 488 nm laser). (iii) Merged bright field images of CellMask Deep Red Plasma and **4a**. b) Confocal fluorescence images of HeLa (row 1), HCT116 (row 2), and MDA-MB-231 (row 3) cells. Images of (i) MitoTracker Red FM (1.0 nM, excited with 561 nm laser), (ii) **4a** (excited with 488 nm laser). (iii) Merged bright field images of MitoTracker and **4a**.

In conclusion, we have designed and synthesized diazapentabenzocorannulenium **4** by 1,3-dipolar cycloaddition of polycyclic aromatic azomethine ylide and 6-chlorophenathridine, followed by palladium-catalyzed intramolecular cyclization. In the crystal state, the obtained buckybowl exhibits a bowl-shaped structure and forms charge-segregated one-dimensional columns by bowl-in-bowl interaction. Despite the lack of hydrophilic substituents, the molecule shows high

water dispersibility and biocompatibility, and thus was applied as a fluorescent cellular probe: **4a** was selectively introduced into the mitochondria of tumor cells. The present study provides an excellent polycyclic aromatic molecular platform which could be utilized for a wide range of applications in material and biological sciences.

Acknowledgements

This work was supported by Nanyang Technological University. B.X. acknowledges the financial support from MOE Tier 1 RG6/20, A*Star SERC A1983c0028, and A20E5c0090. The NTU Center of High Field NMR in SPMS for NMR analyses and the NTU High Performance Computing Team for computing resources are also acknowledged. We thank Dr. Jingjie Ge (MSE, NTU) for TEM analyses.

Conflict of Interest

The authors declare no conflict of interest.

Keywords: Buckybowl · Corannulene · Imidazolium · Fluorescent probe · Mitochondria

[1] Y.-T. Wu, J. S. Siegel, *Chem. Rev.* **2006**, *106*, 4843–4867.
[2] V. M. Tsefrikas, L. T. Scott, *Chem. Rev.* **2006**, *106*, 4868–4884.
[3] W. Jiang, Y. Li, Z. Wang, *Chem. Soc. Rev.* **2013**, *42*, 6113–6127.
[4] A. Narita, X.-Y. Wang, X. Feng, K. Müllen, *Chem. Soc. Rev.* **2015**, *44*, 6616–6643.
[5] X. Y. Wang, X. Yao, K. Müllen, *Sci. China Chem.* **2019**, *62*, 1099–1144.
[6] J. Wu, W. Pisula, K. Müllen, *Chem. Rev.* **2007**, *107*, 718–747.
[7] Q. Miao, *Adv. Mater.* **2014**, *26*, 5541–5549.
[8] G. Hong, S. Diao, A. L. Antaris, H. Dai, *Chem. Rev.* **2015**, *115*, 10816–10906.
[9] X. Li, D. Sun, X. Li, D. Zhu, Z. Jia, J. Jiao, K. Wang, D. Kong, X. Zhao, L. Xu, Q. Zhao, D. Chen, X. Feng, *Biomater. Sci.* **2017**, *5*, 849–859.
[10] J. Wu, J. Li, U. Kolb, K. Müllen, *Chem. Commun.* **2006**, 48–50.
[11] M. Yin, J. Shen, W. Pisula, M. Liang, L. Zhi, K. Müllen, *J. Am. Chem. Soc.* **2009**, *131*, 14618–14619.
[12] E. Nestoros, M. C. Stuparu, *Chem. Commun.* **2018**, *54*, 6503–6519.
[13] H.-A. Lin, Y. Sato, Y. Segawa, T. Nishihara, N. Sugimoto, L. T. Scott, T. Higashiyama, K. Itami, *Angew. Chem. Int. Ed.* **2018**, *57*, 2874–2878; *Angew. Chem.* **2018**, *130*, 2924–2928.
[14] B. M. White, Y. Zhao, T. E. Kawashima, B. P. Branchaud, M. D. Pluth, R. Jasti, *ACS Cent. Sci.* **2018**, *4*, 1173–1178.
[15] S. Ma, Y. Zhu, W. Dou, Y. Chen, X. He, J. Wang, *Sci. China Chem.* **2021**, *64*, 576–580.
[16] Y. Wang, H. Jiang, X. Liu, J. Xu, Y. Gao, N. S. Finney, *Chem. Commun.* **2021**, *57*, 5818–5821.
[17] K. Kawasumi, Q. Zhang, Y. Segawa, L. T. Scott, K. Itami, *Nat. Chem.* **2013**, *5*, 739–744.
[18] N. Ohtsuka, M. Nakano, S. Nakagawa, M. Shahiduzzaman, M. Karakawa, T. Taima, M. Minoura, *Chem. Commun.* **2020**, *56*, 12343–12346.
[19] I. R. Márquez, S. Castro-Fernández, A. Millán, A. G. Campaña, *Chem. Commun.* **2018**, *54*, 6705–6718.
[20] M. Saito, H. Shinokubo, H. Sakurai, *Mater. Chem. Front.* **2018**, *2*, 635–661.
[21] A. D. Buckingham, *Discuss. Faraday Soc.* **1957**, *24*, 151–157.
[22] M. Stępień, E. Gońka, M. Żyła, N. Sprutta, *Chem. Rev.* **2017**, *117*, 3479–3716.
[23] Q. Tan, P. Kaewmati, S. Higashibayashi, M. Kawano, Y. Yakiyama, H. Sakurai, *Bull. Chem. Soc. Jpn.* **2018**, *91*, 531–537.
[24] M. Hirai, N. Tanaka, M. Sakai, S. Yamaguchi, *Chem. Rev.* **2019**, *119*, 8291–8331.
[25] X.-Y. Wang, X. Yao, A. Narita, K. Müllen, *Acc. Chem. Res.* **2019**, *52*, 2491–2505.
[26] W. Wang, X. Shao, *Org. Biomol. Chem.* **2021**, *19*, 101–122.
[27] S. Wang, X. Li, X. Hou, Y. Sun, X. Shao, *Chem. Commun.* **2016**, *52*, 14486–14489.
[28] S. Higashibayashi, P. Pandit, R. Haruki, S. Adachi, R. Kumai, *Angew. Chem. Int. Ed.* **2016**, *55*, 10830–10834; *Angew. Chem.* **2016**, *128*, 10988–10992.
[29] H. Yokoi, S. Hiroto, H. Shinokubo, *J. Am. Chem. Soc.* **2018**, *140*, 4649–4655.
[30] K. Oki, M. Takase, S. Mori, A. Shiotari, Y. Sugimoto, K. Ohara, T. Okujima, H. Uno, *J. Am. Chem. Soc.* **2018**, *140*, 10430–10434.
[31] L. Đorđević, C. Valentini, N. Demitri, C. Mézière, M. Allain, M. Sallé, A. Folli, D. Murphy, S. Mañas-Valero, E. Coronado, D. Bonifazi, *Angew. Chem. Int. Ed.* **2020**, *59*, 4106–4114; *Angew. Chem.* **2020**, *132*, 4135–4143.
[32] A. Babič, S. Pascal, R. Duwald, D. Moreau, J. Lacour, E. Allémann, *Adv. Funct. Mater.* **2017**, *27*, 1701839.
[33] C. Bauer, R. Duwald, G. M. Labrador, S. Pascal, P. M. Lorente, J. Bosson, J. Lacour, J.-D. Rochaix, *Org. Biomol. Chem.* **2018**, *16*, 919–923.
[34] H. Gotoh, S. Nakatsuka, H. Tanaka, N. Yasuda, Y. Haketa, H. Maeda, T. Hatakeyama, *Angew. Chem. Int. Ed.* **2021**, *60*, 12835–12840; *Angew. Chem.* **2021**, *133*, 12945–12950.
[35] Z. Lei, B. Chen, Y.-M. Koo, D. R. MacFarlane, *Chem. Rev.* **2017**, *117*, 6633–6635, and references cited therein.
[36] R. L. Vekariya, *J. Mol. Liq.* **2017**, *227*, 44–60.
[37] S. K. Singh, A. W. Savoy, *J. Mol. Liq.* **2020**, *297*, 112038.
[38] W. A. Herrmann, C. Köcher, *Angew. Chem. Int. Ed. Engl.* **1997**, *36*, 2162–2187; *Angew. Chem.* **1997**, *109*, 2256–2282.
[39] P. de Frémont, N. Marion, S. P. Nolan, *Coord. Chem. Rev.* **2009**, *253*, 862–892.
[40] M. N. Hopkinson, C. Richter, M. Schedler, F. Glorius, *Nature* **2014**, *510*, 485–496.
[41] P. Gandeepan, C.-H. Cheng, *Chem. Asian J.* **2016**, *11*, 448–460.
[42] C. Dutta, J. Choudhury, *RSC Adv.* **2018**, *8*, 27881–27891.
[43] T. van Dijk, S. Burck, M. K. Rong, A. J. Rosenthal, M. Nieger, J. C. Slootweg, K. Lammertsma, *Angew. Chem. Int. Ed.* **2014**, *53*, 9068–9071; *Angew. Chem.* **2014**, *126*, 9214–9217.
[44] K. P. Kawahara, W. Matsuoka, H. Ito, K. Itami, *Angew. Chem. Int. Ed.* **2020**, *59*, 6383–6388; *Angew. Chem.* **2020**, *132*, 6445–6450.
[45] S. Ito, Y. Tokimaru, K. Nozaki, *Angew. Chem. Int. Ed.* **2015**, *54*, 7256–7260; *Angew. Chem.* **2015**, *127*, 7364–7368.
[46] B. W. Laursen, F. C. Krebs, M. F. Nielsen, K. Bechgaard, J. B. Christensen, N. Harrit, *J. Am. Chem. Soc.* **1998**, *120*, 12255–12263.
[47] D. Wu, W. Pisula, V. Enkelmann, X. Feng, K. Müllen, *J. Am. Chem. Soc.* **2009**, *131*, 9620–9621.
[48] Y. Bando, Y. Haketa, T. Sakurai, W. Matsuda, S. Seki, H. Takaya, H. Maeda, *Chem. Eur. J.* **2016**, *22*, 7843–7850.
[49] M. Yamada, S. Tashiro, R. Miyake, M. Shionoya, *Dalton Trans.* **2013**, *42*, 3300–3303.
[50] Y. Haketa, K. Urakawa, H. Maeda, *Mol. Syst. Des. Eng.* **2020**, *5*, 757–771.
[51] S. H. Mahadevegowda, M. C. Stuparu, *Eur. J. Org. Chem.* **2017**, 570–576.

[52] A. Aracena, M. C. Rezende, M. V. Encinas, C. Vergara, S. O. Vásquez, *New J. Chem.* **2017**, *41*, 14589–14594.
[53] U. Rösch, S. Yao, R. Wortmann, F. Würthner, *Angew. Chem. Int. Ed.* **2006**, *45*, 7026–7030; *Angew. Chem.* **2006**, *118*, 7184–7188.
[54] M. P. Murphy, *Biochim. Biophys. Acta Bioenerg.* **2008**, *1777*, 1028–1031.
[55] A. Andrés, M. Rosés, C. Ràfols, E. Bosch, S. Espinosa, V. Segarra, J. M. Huerta, *Eur. J. Pharm. Sci.* **2015**, *76*, 181–191.
[56] H. Wang, B. Fang, B. Peng, L. Wang, Y. Xue, H. Bai, S. Lu, N. H. Voelcker, L. Li, L. Fu, W. Huang, *Front. Chem.* **2021**, *9*, 683220.

Manuscript received: September 16, 2021
Accepted manuscript online: December 4, 2021
Version of record online: December 10, 2021